ACS APPLIED MATERIALS & INTERFACES

Research Article

www.acsami.org

Fabrication of Reduced Graphene Oxide and Sliver Nanoparticle Hybrids for Raman Detection of Absorbed Folic Acid: A Potential Cancer Diagnostic Probe

Chaofan Hu,[†] Yingliang Liu,*[,‡] Jinlan Qin,[†] Guangting Nie,[§] Bingfu Lei,[‡] Yong Xiao,[‡] Mingtao Zheng,[‡] and Jianhua Rong*[,§]

[†]Department of Chemistry and [§]Department of Material Science and Engineering, Jinan University, Guangzhou 510632, P. R. China

[‡]College of Science, South China Agricultural University, Guangzhou 510642, P. R. China

Supporting Information

ABSTRACT: Reduced graphene oxide (RGO) and silver nanoparticle (AgNP) hybrids (RGO-AgNP) were prepared by a facile one-pot method using Poly (N-vinyl-2-pyrrolidone) as reductant and stabilizer. Folic acid (FA) molecules were attached to the RGO-AgNP by physisorption for targeting specific cancer cells with folate receptors (FRs) and using as Raman reporter molecules. The internalization of the FA loaded RGO-AgNP (RGO-AgNP-FA) inside the FRs-positive cancer cell was confirmed by confocal laser scanning and transmission electron microscopy. The Raman signals of the FA in live cancer cells were detected by confocal Raman spectroscope at 514 nm excitation, indicating that the RGO-AgNP-FA material has great potential as a Raman probe for cancer diagnosis in vitro.

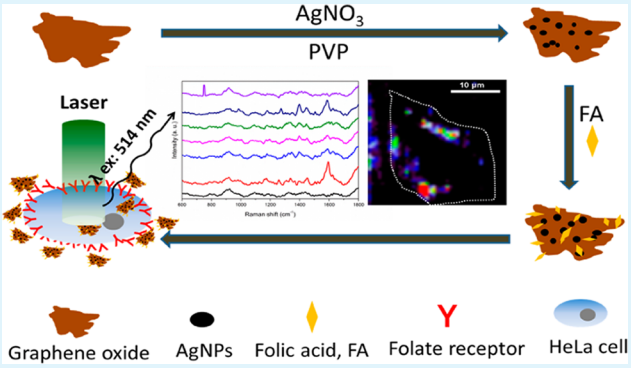

KEYWORDS: *graphene oxide, silver nanoparticle, folic acid, surface-enhanced Raman scattering, cancer, diagnosis*

1. INTRODUCTION

Raman spectroscopy has been widely used in various biomedical applications, because it can provide detailed information about the chemical composition of cells and tissues.[1] Surface-enhanced Raman scattering (SERS), a technique that enhances Raman scattering by molecules adsorbed on rough metal surface, has attracted considerable attention in a number of applications, such as high power superluminescent light-emitting diodes,[2−4] single molecule detection,[5] and biosensors.[6] Apart from sensitive detection of analytes, SERS enables the construction of optical probes using enhanced Raman signals as spectroscopic signature. SERS probes are made with hybrids which typically contain metal (e.g., silver or gold) nanoparticles and reporter molecules. Depending on the specific application, SERS probes can be functionalized with certain antibodies, peptides, and DNA.[7] Over the past decade, new SERS probes have been developed for imaging, and detecting biomarkers and cancers of various organs such as esophagus, breast, lung, bladder, and skin.[8] However, it is still very challenging to fabricate SERS probe functioned with nonthiolated molecules, because these molecules have very low affinity to plasmonic metals.[9]

Graphene oxide (GO) has several oxygen-containing functional groups (e.g., epoxy, hydroxyl, and carboxyl groups), which endow GO with high negative charge and high water solublity as well as capability to easily undergo further modification. Previous studies have shown that GO was a promising candidate in biotechnology.[10] GO and its reduced form, reduced graphene oxide (RGO), have been frequently modified via noncovalent physisorption of small aromatic molecules onto their basal planes through $\pi-\pi$ stacking. These modified GO and RGO have found a wide range of applications such as photothermal cancer therapy,[11−13] drug delivery,[14−16] pollutant management,[17,18] and SERS.[19] Previous studies also showed that GO and RGO were perfect support for various metal nanoparticles such as Au, Ag, Pt, and Pd.[20] There have been many attempts in making GO or RGO hybrids by incorporating certain metal nanoparticles so as to improve the electronic, catalytic and optical properties.[21−23] For example, in the past GO and silver nanoparticle (AgNP) hybrids have been developed for a series of SERS applications,[24−27] The GO and AgNP hybrids also have exhibited improved SERS performance in adsorbing molecules, compared to the traditional silver colloids.[25] Hence, it is anticipated that RGO and AgNP hybrids can be used as SERS-active material, in which AgNP can enhance Raman scattering while RGO can concentrate the reporter molecules with its high adsorption capacity.

Folic acid (FA) is a vitamin that is essential for proliferation and maintenance of all cells. Many cancers express high levels of folate receptors (FRs), for example, cancers of ovary, lung,

Received: January 6, 2013
Accepted: April 29, 2013
Published: April 29, 2013

 © 2013 American Chemical Society dx.doi.org/10.1021/am4000485 | ACS Appl. Mater. Interfaces 2013, 5, 4760−4768

kidney, breast, brain, and colon.[28] FA or FA-containing nanomaterials have been designed to target cancer cells, as the FA has very high affinity to the FRs in these cancer cells. For example, graphene-based drug delivery materials have been prepared to target cancer cells by covalent binding of FA to surface of GO or RGO.[16,29] Although using this covalent binding method can produce relatively stable materials, it is very difficult to practice the method due to the many challenges related to the corresponding process such as the potentially dangerous acid condition, long reaction time and additional purification steps, and high cost.[30] In addition, covalent binding may produce toxic by-product and hinder recognition by FRs.[31] Graphene can also be functionalized via non-covalent binding such as $\pi-\pi$ stacking, cation$-\pi$, and van der Waals interactions in biological applications.[32] In contrast to covalent binding, noncovalent modification is considered to have less impact on the conjugated structure, and the mechanical and electrical properties of graphene.[33] Ren et al. demonstrated that the enrichment and ultrasensitive detection of FA can be achieved by using GO and AgNP hybrids in human serum, indicating that the influence of the remaining protein in serum was negligible during the detecting process.[25] FA can be internalized by FR-positive cancer cells, which first internalize a FA molecule captured by an FR, and then send the FR back to the cell surface to capture more FA. This FR-mediated endocytosis mechanism also applies when FA is tethered to a nanoparticle.[29] For example, previous study showed that even when FA was noncovalently bonded on single-walled carbon nanotubes (SWCNTs), it still could be internalized by FR-positive THP-1 cells through interaction with the FRs.[30] Lee et al. found that by noncovalently binding FA to polyethylenimine/DNA polyplex, the DNA transfection could be greatly enhanced in a variety of cell lines.[34] With such effect, this FA modification approach may provide a reliable, low-cost, and highly efficient way to deliver genes, and therefore may find applications in gene therapy.[34] In this paper, we developed a simple and efficient SERS probe for cancer diagnosis with RGO and AgNP hybrids loaded with FA (RGO-AgNP-FA), as shown in Figure 1. We also used the probe for Raman detection of

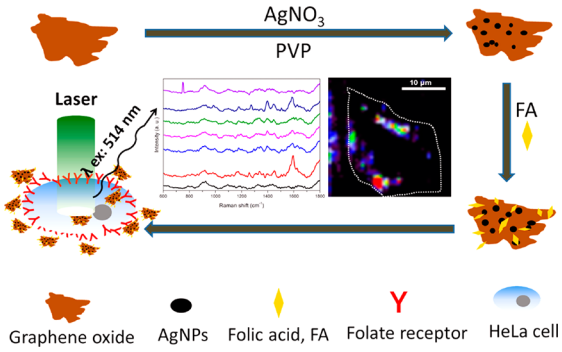

Figure 1. Schematic illustration of fabrication of RGO-AgNP-FA as a SERS probe for cancer diagnostics in vitro.

FRs-positive cancer cells. To the best of our knowledge, it is the first time that FA was used as both the Raman reporter molecule and the targeting ligand for cancer cells. This probe was fabricated through three main steps. First, GO was prepared with native graphite flake according to the modified Hummer's method. Then, AgNPs were loaded on the surface of GO as the hot spots for generating strong SERS signals. Finally, FA was attached to the surface of RGO-AgNP by physisorption. To investigate the targeting performance of the probe, we used HeLa cells as model cancer cells because they over-express the FRs (FRs-positive), and A549 cells were used as control because they express few FRs (FRs-negative). The cellular uptake of the nanomaterials was studied by confocal laser scanning microscope (CLSM) and transmission electron microscopy (TEM) observation of the cancer cells incubated with RGO-AgNP-FA. The Raman signals of FA were successfully detected with confocal Raman spectroscope in live HeLa cells, while the signals cannot be observed in A549 cells, demonstrating the efficient targeting ability of RGO-AgNP-FA and also the potential application of the RGO-AgNP-FA material as a Raman probe for cancer diagnosis in vitro.

2. METHODS AND MATERIALS

2.1. Materials. Graphite was purchased from Alfa Aesar. Poly (N-vinyl-2-pyrrolidone) (PVP, K30, molecular weight = 30 000−40 000 g/mol) was obtained from Shanghai Chemical Factory. Silver nitrate and FA were purchased from Beijing Chemical Reagent Factory. Dulbecco's modified Eagle's medium (DMEM), 3-(4,5-dimethylthiazol-2-yl)-2,5-dipheny-ltetrazolium bromide (MTT), heat-inactivated newborn calf serum, trypsin, penicillin, and streptomycin were purchased from Gibco Invitrogen. All reagents were analytical grade and used as received without further purification. All aqueous solutions were prepared with Milli-Q water (>18.2 MΩ cm) from a Milli-Q Plus system (Millipore).

2.2. Synthesis of GO. GO was prepared from native graphite flake according to the modified Hummer's method.[35,36] The GO sample was then dried in a vacuum oven at 25 °C overnight. To prepare single-layer GO sheet, GO was first cracked with an ultra-sonic probe operating at 600 W for 2 h. The resulted brown dispersion was then subjected to centrifugation at 10 000 rpm for 20 min so as to remove any unexfoliated graphite oxide. Finally, a homogeneous aqueous GO dispersion (about 0.5 mg/mL) was obtained.

2.3. Synthesis of RGO-AgNP. RGO-AgNP was prepared according to the reported method with some minor modifications.[24] In a typical procedure, 3.76 g of PVP was dissolved in 16 mL of GO aqueous solution, and the solution was then heated to 60 °C in air under magnetic stirring. Afterwards, 12 mL of a $AgNO_3$ aqueous solution (188 mM) was rapidly added into the above solution, and stirring was continued for 5 min to ensure complete mixing. Next, the reaction was allowed to proceed without agitation for 48 h at 60 °C. The RGO-AgNP product was then centrifuged at 8000 rpm for 20 min and washed with Milli-Q water to remove excess PVP. Finally, the purified RGO-AgNP was redispersed into 5 mL of phosphate-buffered saline (PBS) solution (pH 7.4) via sonication for further use.

2.4. Synthesis of RGO-AgNP-FA. Loading FA on RGO-AgNP was achieved by mixing RGO-AgNP with FA (1×10^{-4} M) in PBS solution at room temperature for 24 h followed by repeated washing to remove unbound FA. The RGO-AgNP-FA was then redispersed into PBS solution for further use.

2.5. Characterization of Hybrids. The morphology feature of the AgNPs and RGO-AgNP-FA were characterized with a Philips TECNAI 10 transmission electron microscope and a JEOL JEM-2100F field emission electron microscope equipped with an Oxford INCA Energy TEM 200 EDS system. UV-Vis spectra were obtained with a Varian Cary 5000 UV−vis spectrophotometer. The crystallographic phases of the products were examined by XRD using a Bruker D8-Advance powder X-ray diffractometer with Cu Kα radiation (λ = 0.15418 nm). Atomic force microscopy (AFM) images were taken in tapping mode with the SPM Dimension 3100 from Veeco. The Raman spectra of the samples were measured with a Renishaw inVia microspectrometer using an excitation wavelength of 514 nm generated by an Ar^+ laser. A 100× objective was used to focus the laser beam and also collect the Raman signal. The lateral resolution of the instrument was about 1 μm, and the laser power on sample was about 0.1 mW to avoid laser-induced heating. Before each data

dx.doi.org/10.1021/am4000485 | ACS Appl. Mater. Interfaces 2013, 5, 4760−4768

acquisition, the intensity of the Raman peak at 520 cm^{-1} from silicon was normalized, and the Raman spectra were then recorded in the range of 550−1800 cm^{-1} during a 30 s acquisition. The peak intensity was obtained by fitting it with the Lorentzian function.

2.6. Cell Culture and Viability Measurements. HeLa cells were cultured in Dulbecco's modified Eagle medium (DMEM) supplemented with 10% heat-inactivated newborn calf serum, and 1% penicillin−streptomycin under a humidified atmosphere (5% CO_2 plus 95% air) at 37 °C. The effect of RGO-AgNP-FA on cell proliferation was investigated by MTT assay. First, HeLa cells were seeded onto 96-well plates (5×10^3 cells per well) and incubated for 24 h. Then, RGO-AgNP-FA was introduced to the cells with a predetermined concentration in the culture medium (12.5, 25, 50, or 100 μg/mL). After 24, 48, or 72 h incubation, the medium was replaced by a solution of MTT, and the cells were incubated for another 4 h. The reaction was terminated by adding 150 μL of DMSO after removing the supernatant medium. When the purple formazan crystals were resolved by DMSO, the absorbances of the wells were measured with a Bio-Rad ELISA reader at 570 nm. Cells incubated in the absence of RGO-AgNP-FA were used as a control.

2.7. Cellular Uptake and Internalization. To investigate the cellular uptake of RGO-AgNP-FA by means of CLSM, Rho B was used to label the RGO-AgNP-FA by physical adsorption. The same method has been described elsewhere for studying the cellular uptake of GO in drug delivery.[11,16] The complexes of RGO-AgNP-FA-Rho B were formed by simply mixing of RGO-AgNP-FA with Rho B for 24 h at room temperature and then repeatedly washing to remove unbound Rho B. HeLa and A549 cells (1×10^4 per well) growing in 35 mm Petri dishes were incubated with a RGO-AgNP-Rho B suspension (50 μg/mL) for 2 h, and then rinsed with PBS solution and fixed with glutaraldehyde in 4-(2-hydroxyethyl)-1-piperazineethanesulfonic acid (HEPES) buffer (pH 7.4). The fluorescence emission from Rho B was measured by CLSM (LSM 510/ConfoCor 2 META) combination system (Zeiss, Jena, Germany) equipped with a Plan-Neofluar 40×/1.3 NA Oil DIC objective. Rho B was excited at 543 nm with a He−Ne laser, and the emitted light was recorded through a 600 nm long-pass filter. The in-situ TEM observation of RGO-AgNP-FA in cells was performed with a Philips TECNAI 10 transmission electron microscope operated at 100 kV. The HeLa cells were incubated with RGO-AgNP-FA (50 μg/mL) for 2 h, and then washed in PBS solution, pelleted by centrifugation, and then fixed for 2 h in 3% glutaraldehyde in HEPES buffer (pH 7.4). After the cells were dehydrated and embedded in Epoxy 618, the ultrathin sections were cut with an EM-UC6 microtome (Leica, Germany), then stained with uranyl acetate and lead citrate prior to examination with TEM.

2.8. SERS Detection of FA in Live Cancer Cells. To detect RGO-AgNP-FA in cells via SERS, HeLa cells and A549 cells were seeded into sterile glass coverslips culture petri dishes (35 mm) and incubated for 24 h, the culture medium was then replaced by a culture medium containing RGO-AgNP-FA (50 μg/mL) and incubated for another 2 h at 37 °C. Before measurement, the culture dishes were washed with fresh PBS solutions three times to remove any unbound RGO-AgNP-FA. An excitation wavelength at 514 nm, 50% laser intensity, and overlaying twice with 10 s integration time were the conditions used for testing live cancer cells with confocal Raman spectroscope. Raman imaging was performed by using a Renishaw inVia confocal Raman system (controlled by WiRE 3.2 software) coupled to a Leica DM2500 microscope. Raman spectral mapping was performed in Renishaw's StreamLine rapid Raman imaging system at 10 s integration time (~2 s per pixel) at a wave number center of 1590 cm^{-1}. Raman images were generated using the integrated signal-to-baseline intensity from 1200 to 1800 cm^{-1}. To ensure the FA-FRs interaction, one control experiment was conducted as described in the reference.[37] In this control experiment, HeLa cells on culture dishes were first treated with free FA (0.5 mg/mL) for 2 h to saturate the FRs, followed by another 2 h of RGO-AgNP-FA treatment. Then, the treated culture dishes were washed with fresh PBS solutions three times to remove any unbound RGO-AgNP-FA.

3. RESULTS AND DISCUSSION

3.1. Characterization of RGO-AgNP. The morphology of GO and RGO-AgNP were investigated by TEM. As shown in Figure 2A, the GO sheets are less than 500 nm in lateral

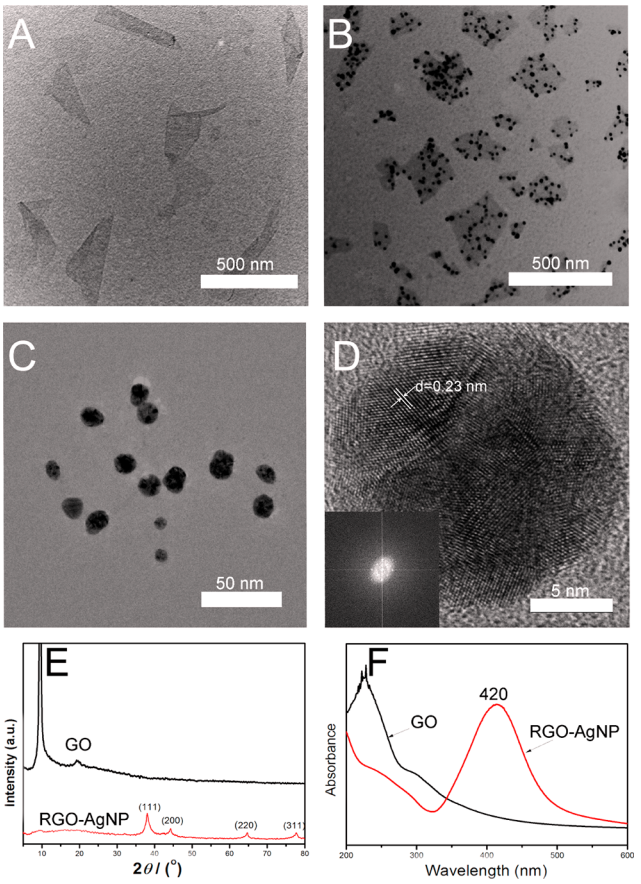

Figure 2. Charaterization of GO and RGO-AgNP. (A) TEM image of GO. (B, C) TEM images of RGO-AgNP under different magnifications. (D) HRTEM image and (inset) corresponding FFT analysis of Ag NP; (E, F) XRD pattern and UV−vis spectra of GO and RGO-AgNP.

dimension. The TEM image of RGO-AgNP (Figure 2B, C) shows that the almost-transparent GO sheets are decorated with large amounts of well-dispersed AgNPs. In addition, almost all of the AgNPs are confined within the GO sheets, and very few AgNPs reside outside the GO support. This implies that the interaction between the AgNP and GO is strong. The size of AgNPs ranges from 5 to 20 nm with an average 13 nm. The high-resolution TEM (HRTEM) images (Figure 2D) indicate that the AgNP adsorbed on the GO surface is a multicrystalline particle. The measured interplanar spacing for the lattice fringes is 0.23 nm, which corresponds to the (111) lattice plane of Ag.[38] From the AFM image of RGO-AgNP on the mica (Figure S1), the thickness of the RGO sheet is measured to be about 1 nm, which indicates that the RGO is a monolayer sheet. After loading AgNPs, the thickness of RGO-AgNP increases to about 14 nm, suggesting that the AgNPs are adsorbed on to the surface of the GO sheets. The formation of RGO-AgNP was further characterized by X-ray diffraction (XRD) (Figure 2E). Compared with the GO, the XRD pattern of RGO-AgNP shows obvious peaks corresponding to the (111), (200), (220), and (311) diffraction peaks of fcc Ag,

dx.doi.org/10.1021/am4000485 | ACS Appl. Mater. Interfaces 2013, 5, 4760−4768

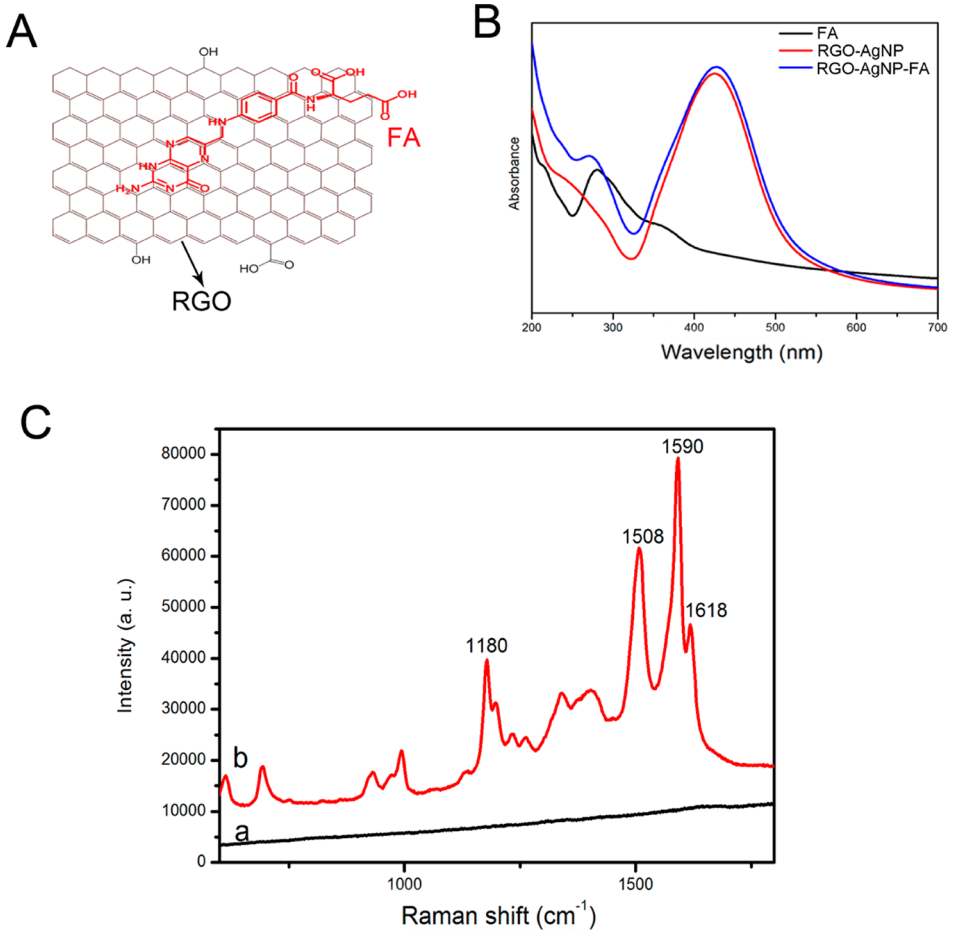

Figure 3. (A) Schematic illustration of the interaction of the FA molecular with the RGO surface. (B) UV−vis spectra of FA, RGO-AgNP, and RGO-AgNP-FA. (C) Raman spectra of (a) FA (1×10^{-4} M) and (b) RGO-AgNP-FA in PBS solution.

which confirms that AgNPs exist in crystalline state.[24] The binding of GO with AgNPs is also supported by UV−vis spectral analysis. As shown in Figure 2F, GO displays a maximum absorption peak centered at 230 nm and a shoulder peak at about 300 nm. After attachment with Ag NPs onto the GO surface and reduction by PVP, a new peak at about 420 nm is clearly seen. This is attributed to the surface plasmon absorption of AgNPs, representing another evidence of the formation of RGO-AgNP. Raman spectroscopy shown in Figure S2 in the Supporting Information reveals the Raman signal enhancement for RGO-AgNP, which was consistent with the SERS effect previously reported in metal−graphene structures,[39,40] indicating the strong interaction of AgNPs with RGO. Such strong adsorption of AgNPs onto the GO can be explained by the presence of carboxyl, hydroxyl and epoxy groups in GO, which are possible nucleation sites for anchoring AgNPs. This theory has been discussed for such adsorption.[41] It was observed that the growth of small AgNPs was related to the amount of oxygenated functional groups on GO.[20,42] Theoretical calculations suggested that the silver or gold nanoparticles bind to graphene surfaces through dispersion and charge-transfer interactions while the palladium nanoparticles bind by dative bonds.[43] PVP has been reported to reduce both the silver nitrate and GO simultaneously at 60 °C.[24] As shown in Figure S2 in the Supporting Information, RGO-Ag formed by PVP reduction exhibits two characteristic main peaks at 1365 and 1594 cm^{-1}, which can be ascribed to the D and G bands of graphene. Compared with GO, the G band of RGO-Ag red-shifts from 1605 to 1594 cm^{-1}, which confirms that GO are successfully reduced.[24] PVP is an excellent low-cost and biocompatible dispersion agent. Previous reports showed that addition of PVP could remarkably improve solubility of graphene and RGO in water. PVP-protected graphene-based materials have been widely applied in biosensing.[44,45] PVP was used as the reductant and stabilizer in the preparation of RGO-AgNP in this paper. Even after multiple centrifugal washing of the RGO-AgNP to remove excess PVP, some PVP still absorbed on the surface of GO, serving as the surfactant to prevent the aggregation of composites.

3.2. FA Loading and SERS Detection. FA, which was attached to the surface of RGO-AgNP by physisorption, was used as both the Raman probe molecule and the targeting ligand for cancer cells. Previous studies reported that FA could be attached to the surface of GO or RGO by either electrostatic adsorption[25] or covalent interaction.[29] In this study, we attributed the interaction of FA with RGO-AgNP to non-covalent physisorption of small aromatic molecules onto the RGO surface by $\pi-\pi$ stacking (Figure 3A). The absorption band at 270 nm for FA is attributed to the transition $\pi-\pi^*$ bond in carboxylate.[46] After absorbed on the RGO surface, a blue-shift of FA peak from 282 nm to 270 nm was observed (Figure 3B), which is similar as a previous observation regarding the single-walled carbon nanotube-FA conjugates by noncovalent interaction.[30] As shown in Figure 3C, strong

dx.doi.org/10.1021/am4000485 | ACS Appl. Mater. Interfaces 2013, 5, 4760−4768

signals of FA in the SERS spectra (b in Figure 3C) are recorded when there is RGO-AgNP in PBS solution. The main vibrations of FA in SERS spectra with RGO-AgNP in PBS solution have four strong peaks (1180, 1508, 1590, and 1618 cm^{-1}), which are consistent with the reported work.[25,47] These characteristic peaks providing the information of the molecules could be used to identify FA in the cells. In contrast, no Raman peaks can be observed with the absence of RGO-AgNP under the same experimental conditions (a in Figure 3C). There are two causes for this difference: (1) RGO concentrated the FA molecules; and (2) the AgNPs adsorbed on the surface of RGO enhanced the Raman signals of FA due to their great electromagnetic effect. Therefore, a strong SERS spectrum of FA was observed with the RGO-AgNP, leading to an ultrasensitive detection of FA. These enhanced Raman signals of FA could be used to identify FA in certain cancer cells by using RGO-AgNP-FA as diagnostic probe materials, which will be discussed later. To further investigate the interaction between RGO-AgNP and aromatic molecules, crystal violet (CV) was chosen as another SERS reporter molecules. As shown in Figure S3 in the Supporting Infomration, the strong SERS signals of CV are also observed after loading on the surface of RGO-AgNP. Clearly, the RGO-AgNP material has excellent SERS performance for nonthiolated aromatic molecules. Such great enhancement of the Raman signals of non-thiolated aromatic molecules in aqueous solution can be explained by both the great electromagnetic effect of AgNPs and the strong adsorption capacity of RGO for aromatic molecules by $\pi-\pi$ stacking.

3.3. In Vitro Cytotoxicity Study. It was found that RGO-AgNP-FA materials exhibited excellent stability and solubility in water, PBS solution (pH 7.4) and culture medium (DMEM supplemented with 10% heat-inactivated newborn calf serum, and 1% penicillin–streptomycin). No aggregation was observed in these solutions after a week (see Figure S4 in the Supporting Information). This is due to the strong interactions between RGO sheets and PVP molecules. To show the potential utility of the as-prepared RGO-AgNP-FA as a new cancer diagnostic probe, an in vitro cytotoxicity of RGO-AgNP-FA on cancer cells was determined by using the MTT assay. A time- and dose-dependent approach was employed to evaluate the toxicity of the samples. HeLa cells were incubated with various concentrations of RGO-AgNP-FA for 24, 48, or 72 h. The dependence of the viability of the cells is shown in Figure 4. It has been reported that when contacting the proteins of cells and the phosphorus containing compounds in the cytoplasm, AgNPs could affect the functions of cell respiration and cell growth, resulting in the death of the cells.[48−50] The as-prepared RGO-AgNP-FA showed no significant toxicity on HeLa cells at low concentration (lower than 25 μg/mL) after less than 24h incubation periods. However, with the increasedconcentration of RGO-AgNP-FA and the prolonged incubation time, the materials showed increased cytotoxicity to HeLa cells. No significant toxicity of the as-prepared RGO-AgNP-FA on HeLa cells at low concentration could be due to the low density of AgNPs on the RGO surface. Another possible reason is the improved biocompatibility in the presence of PVP residues since PVP was reported as a good biocompatible capping agent.[51]

3.4. Cellular Uptake and Internalization. FR is a highly selective tumor marker overexpressed in greater than 90% of the ovarian carcinomas.[52] The folate provides one uptake mechanism, through FRs-mediated endocytosis, which first internalizes a FA molecule captured by an FR, then returns the

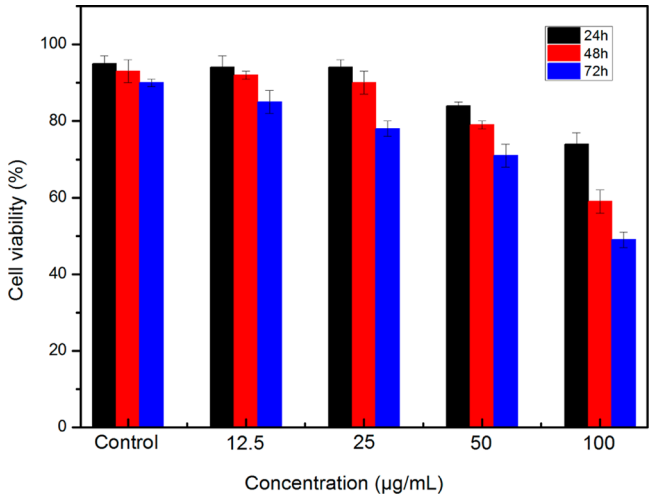

Figure 4. Dose-and time-dependent viability of HeLa cells incubated with different concentration of RGO-AgNP-FA. Each data point represents the mean value from at three independent experiments.

FR to the cell surface to capture more FA.[29] This mechanism also applies when FA is attached to nanoparticles.[53] To understand the cellular uptake of RGO-AgNP-FA by different cells with and without FRs, we used Rho B to label RGO-AgNP-FA by physical adsorption. The cellular uptake of as prepared RGO-AgNP-FA-Rho B was studied using a confocal laser scanning microscope (CLSM). As shown in Figure 5A, an absorption peak appears at about 550 nm, characteristic of Rho B in the UV/vis spectra, which suggests binding of Rho B to RGO-AgNP-FA (Figure 5A). In Figure 5B, fluorescence with a peak at 577 nm (excited at 543 nm) was observed for the

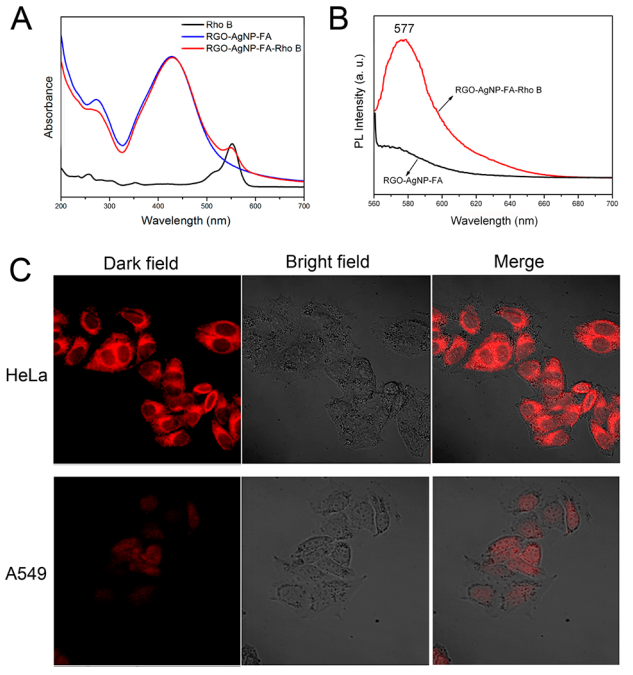

Figure 5. (A) UV–vis spectra of Rho B, RGO-AgNP-FA, and RGO RGO-AgNP-FA- Rho B. (B) Normalized PL spectra of RGO-AgNP-FA and RGO-AgNP-FA- Rho B in PBS solution. (C) fluorescence (left), bright-field (center), and merge (right) images of HeLa cells (top) and A549 cells (down) incubated with RGO-AgNP-FA- Rho B for 2 h.

dx.doi.org/10.1021/am4000485 | ACS Appl. Mater. Interfaces 2013, 5, 4760−4768

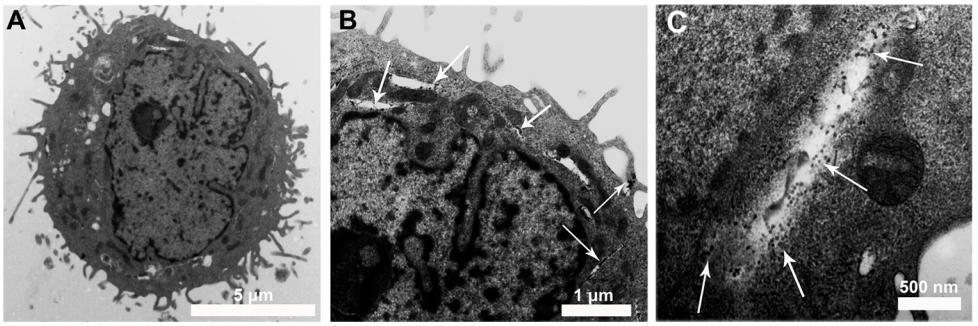

Figure 6. Thin-section TEM images of HeLa cells incubated with 50 μg/mL RGO-AgNP-FA for 2 h. Arrows denote the RGO-AgNP-FA uptaken by the cell.

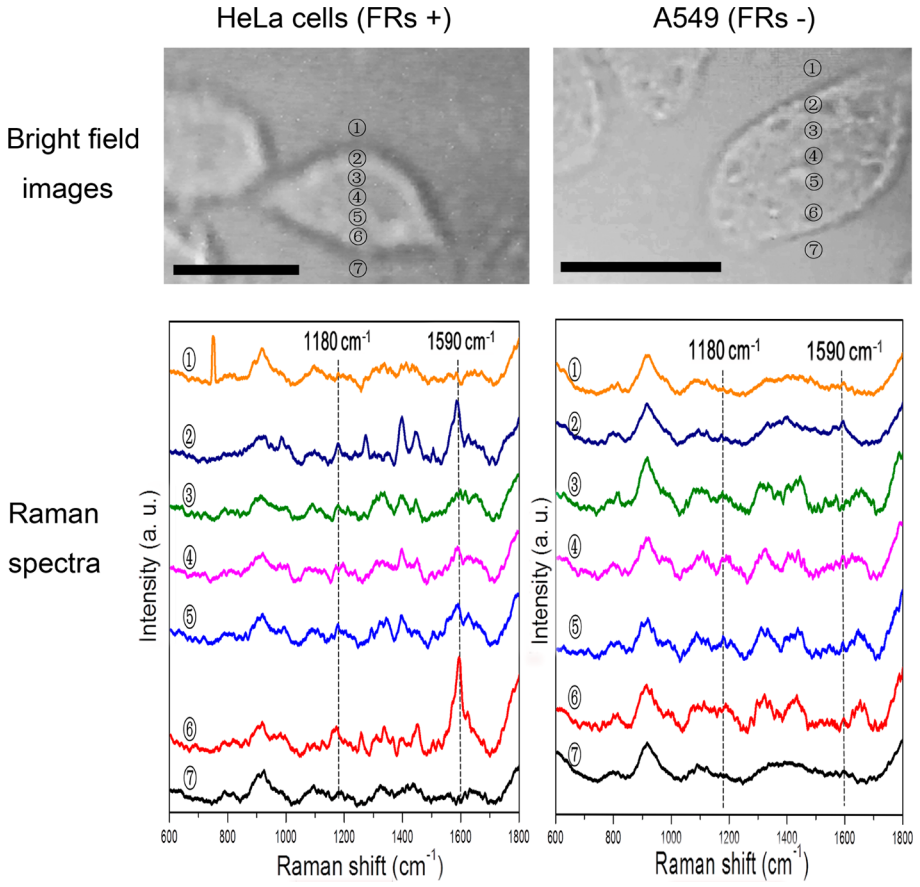

Figure 7. Example bright-field and Raman images for HeLa and A549 cells and corresponding SERS spectra after being incubated with RGO-AgNP-FA. Scale bar, 10 μm. The numbered spots on the bright-field cell images indicate the locations where the laser beam is focused on for SERS measurements.

RGO-AgNP-FA-Rho B dispersed in PBS solution. It is noted that the fluorescence of the RGO-AgNP-FA-Rho B was significantly weaker than that of the free RhoB in PBS solution. This result indicates partial quenching of the fluorescence by adsorption of Rho B onto the surface of RGO-AgNP-FA. The partial fluorescence quenching is due to fluorescence resonance energy transfer from the dye to the RGO, a phenomenon also observed previously for dyes adsorbed onto graphene.[54] To examine the targeting capability of RGO-AgNP-FA as a potential cancer diagnostic probe, we incubated RGO-AgNP-FA-Rho B with HeLa cells (FRs-positive) and A549 cells (FRs-negative) for 2 h and monitored their interactions. The CLSM image (Figure 5C) shows that RGO-AgNP-FA was readily internalized by the HeLa cells and mainly localized in the cytoplasm region. In contrast, the fluorescence on A549 cells was weak after 2 h incubation with RGO-AgNP-FA. The much stronger fluorescence shown in HeLa cells than in A549 cells suggests that HeLa cells had higher uptake of RGO-AgNP-FA than A549 cells. This result demonstrates the targeting capability of RGO-AgNP-FA to the cells with FRs.

To further investigate the cellular uptake and internalization of RGO-AgNP-FA, we also observed the ultrastructure of HeLa cells by TEM. The thin-section TEM images clearly show that the RGO-AgNP-FA is incorporated into HeLa cells after 2 h of incubation. It was reported that the metal nanoparticles had relative high electron density than cellular structures, which could be easily distinguished in the TEM observation.[55,56] As can be seen in Figure 6, the RGO-AgNP-FA materials are

dx.doi.org/10.1021/am4000485 | ACS Appl. Mater. Interfaces 2013, 5, 4760−4768

clearly visible and distinct from the cellular due to their high electron density of AgNPs. After internalization, the RGO-AgNP-FA materials were found to be located in endosomes in the cytoplasm, suggesting a mechanism of receptor-mediated endocytosis via the FRs. It is observed that RGO-AgNP-FA does not show any change in shape and size after being endocytosed in cells (see the white arrows in Figure 6C). Few RGO-AgNP-FA is seen in the nucleus, which is consistent with the fluorescence images (Figure 5). These nanoprobes are believed to able to target FRs on the surface of HeLa cells, therefore be endocytosed via the FRs mediated path in endosomes, and then be distributed in the cytoplasm of HeLa cells. The results from TEM observation are consistent with those from the CLSM image.

3.5. SERS Detection of FA in Live Cancer Cells. The capability for very sensitive Raman detection, along with the fact that the spectral information in SERS only comes from the immediate vicinity of the nanostructures, makes gold and silver nanoprobes based on SERS ideal tools for targeted studies in living biological systems.[57] SERS probes are hybrids consisting of metal nanostructures, typically combinations of silver or gold nanoparticles and reporter molecules. Such probes can be endocytosed by cells and identified by the strong and distinct SERS signals of the attached reporter molecules. In this study, FA molecules were attached to the RGO-AgNP by physisorption for targeting specific cancer cells with FRs and using as Raman reporter molecules. To investigate the performance of RGO-AgNP-FA as a SERS diagnostic probe in vitro, we incubated the hybrids with HeLa and A549 cells and examined by confocal Raman spectroscopy. Figure 7 shows the intracellular Raman spectra of HeLa cells and A549 cells at different laser spots after the incubation with RGO-AgNP-FA. It is obvious that the SERS signals from FA molecules remain robust and are not overwhelmed by a large background after the probes being incorporated into living HeLa cells. The characteristic band of FA at about 1180, 1508, 1590, and 1618 cm^{-1} are clearly observed. By comparing the intensities of Raman signals at the different region of the cell, much stronger SERS signals were observed on the cytoplasm of HeLa cells near the cell membrane than on the nucleus, indicating that RGO-AgNP-FA had been uptaken by the cancer cells and located at the cytoplasm region after 2 h of incubation. This SERS result is consistent with the CLSM and TEM results. On the other hand, the Raman signals of FA are too weak to be distinguished after incubated with FRs-negative A549 cells, demonstrating that few RGO-AgNP-FA were internalized by the cells.

To further study the SERS performance of RGO-AgNP-FA, Raman images are obtained by spatially mapping the cells with the integrated intensity of 1590 cm^{-1}. Although both Raman and fluorescence imagings belong to chemical imaging, they are carried out in different modes in terms of the observation set-up. The former is based on the fluorescence emission, whereas the latter is based on the optical transmission and scattering. Most currently available fluorescent dyes have relatively weak emission intensities and are rapidly photobleached. Thus more sensitive and stable cell imaging techniques are needed. Raman imaging is a more powerful technique that offers picomolar sensitivity, nanoscale resolution and multiplexing capabilities to the field of molecular imaging.[8,58,59] Compared with the fluorescence spectroscopy, Raman imaging provides narrow spectral bandwidth and is resistant to photobleaching and autofluorescence of the biological system, suitable for long-term monitoring of cellular processes.[60] However, the sensitivity of the two methods for cell imaging depends, to a great extent, on the quality of instrument, such as the power of the laser and sensitivity of the charge-coupled device (CCD). From this aspect, conventional fluorescence spectroscopy might be more mature and advanced than the newly developed Raman imaging technique. For example, the acquisition time of a Raman image is still much longer than a fluorescence image. Typical Raman images consist of thousands of individual spectra from which various pieces of information can be extracted in order to display certain chemical information as an image. Acquisition time reduction can be achieved through the optimization of various parts of the confocal Raman microscope. Dieing et al. described the usage of an ultra-high throughput spectrometer in combination with a spectroscopic electron multiplying CCD camera as a detector, which reduces the acquisition time for single Raman spectra to a matter of milliseconds and significantly enhances the sensitivity of the instrument.[61] In this study, the Raman spectral mapping was performed in the Renishaw's StreamLine rapid Raman imaging system to reduce the acquisition time, which allows the collection of a Raman image with 50×50 pixels image resolution in less than 20 min. HeLa Cells incubated with RGO-AgNP-FA for 2 h (Figure 8A)

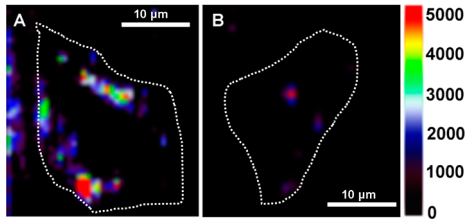

Figure 8. Typical SERS image of (A) HeLa and (B) A549 cells incubated with RGO-AgNP-FA (using the intensity of FA at 1590 cm^{-1}). The dotted lines in the images are drawn to indicate the boundaries of selected cells.

exhibit distinct Raman images because of the weak inherent Raman intensity while the control cells (A549) exhibit weak Raman signals (Figure 8B). Our results clearly show that HeLa cells incubated with RGO-AgNP-FA exhibit significantly enhanced Raman signals of FA and thus more distinguishable Raman images are obtained. Our experimental data with HeLa cells, as well as with A549 cells, clearly demonstrate that our SERS assay is able to distinguish FRs over-expressed cancer cells from the cells on which the FRs are not over-expressed. To further ensure the FA-FR interaction, FR-positive HeLa cells were first treated with free FA to saturate the FA receptors, and then, the cells were treated with RGO-AgNP-FA. In this assay, the HeLa cells were first incubated either with or without free FA in the medium for 2 h, and then, the cells were treated with RGO-AgNP-FA for 2 h. Before the Raman imaging measurement, the culture dishes were washed with PBS solution for three times to remove any unbound RGO-AgNP-FA. Not surprisingly, the uptake of RGO-AgNP-FA is effectively suppressed in the group treated with free FA, as supported Raman imaging (see Figure S5 in the Supporting Information). Such a distinct suppression effect shows that the internalization of RGO-AgNP-FA is hindered due to the reduced availability of FRs on the cell surfaces, in agreement with the previously reported results.[37,62] It further confirms the notion that our probe is able to specifically target FRs on the FRs-positive cancer cells. We believe that this SERS-active

nanomaterial could have enormous potential for application in the diagnosis of FRs-positive tumor in vitro.

4. CONCLUSION

In summary, we reported the synthesis of a functional RGO-AgNP-FA hybrid material with good biocompatibility and targeting ability, and also its application in Raman detecting of live cancer cells. The RGO-AgNP was prepared by a facile one-pot method using PVP as reductant and stabilizer. The as-prepared RGO-AgNP showed great enhancement in the Raman signals of the absorbed FA, which has the potential to target FRs-positive cancer cells and serve as Raman reporter molecule. Cellular uptake experiments demonstrated the efficient and targeted delivery of RGO-AgNP-FA into HeLa cells via receptor-mediated endocytosis. The SERS signals of the FA in FRs-positive cancer cells were successfully detected at 514 nm excitation. The above experimental results indicate that the RGO-AgNP-FA has not only very good targeting capability to live cancer cells but also great potential as a new Raman probe for cancer diagnosis.

■ ASSOCIATED CONTENT

Supporting Information

Additional information as noted in text. This material is available free of charge via the Internet at http://pubs.acs.org.

■ AUTHOR INFORMATION

Corresponding Author

*E-mail: tliuyl@163.com (Y.L.); trong@jnu.edu.cn (J.R.).

Notes

The authors declare no competing financial interest.

■ ACKNOWLEDGMENTS

This work was supported by the National Natural Science Foundation of China (Grant 21031001, 20906037, 20604010, 51173070), the Fundamental Research Funds for the Central Universities (21610102).

■ REFERENCES

(1) Zhang, Y.; Hong, H.; Cai, W. *Curr. Pharm. Biotechnol.* **2010**, *11*, 654−61.
(2) Zang, Z.; Mukai, K.; Navaretti, P.; Duelk, M.; Velez, C.; Hamamoto, K. *Appl. Phys. Lett.* **2012**, *100*, 031108.
(3) Zang, Z.; Minato, T.; Navaretti, P.; Hinokuma, Y.; Duelk, M.; Velez, C.; Hamamoto, K. *IEEE Photonics Technol. Lett.* **2010**, *22*, 721−723.
(4) Zang, Z.; Mukai, K.; Navaretti, P.; Duelk, M.; Velez, C.; Hamamoto, K. *IEICE Trans. Electron.* **2011**, *E94C*, 862−864.
(5) Qian, X. M.; Nie, S. M. *Chem. Soc. Rev.* **2008**, *37*, 912−920.
(6) Notingher, I. *Sensors* **2007**, *7*, 1343−1358.
(7) Matschulat, A.; Drescher, D.; Kneipp, J. *ACS Nano* **2010**, *4*, 3259−3269.
(8) Zhang, Y.; Hong, H.; Myklejord, D. V.; Cai, W. *Small* **2011**, *7*, 3261−3269.
(9) Hering, K.; Cialla, D.; Ackermann, K.; Dorfer, T.; Moller, R.; Schneidewind, H.; Mattheis, R.; Fritzsche, W.; Rosch, P.; Popp, J. *Anal. Bioanal. Chem.* **2008**, *390*, 113−124.
(10) Wang, Y.; Li, Z.; Wang, J.; Li, J.; Lin, Y. *Trends Biotechnol.* **2011**, *29*, 205−212.
(11) Zhang, W.; Guo, Z.; Huang, D.; Liu, Z.; Guo, X.; Zhong, H. *Biomaterials* **2011**, *32*, 8555−8561.
(12) Dai, H. J.; Robinson, J. T.; Tabakman, S. M.; Liang, Y. Y.; Wang, H. L.; Casalongue, H. S.; Vinh, D. *J. Am. Chem. Soc.* **2011**, *133*, 6825−6831.
(13) Liu, Z. A.; Yang, K.; Zhang, S. A.; Zhang, G. X.; Sun, X. M.; Lee, S. T. *Nano Lett.* **2010**, *10*, 3318−3323.
(14) Dai, H. J.; Liu, Z.; Robinson, J. T.; Sun, X. M. *J. Am. Chem. Soc.* **2008**, *130*, 10876−10877.
(15) Yang, X. Y.; Wang, Y. S.; Huang, X.; Ma, Y. F.; Huang, Y.; Yang, R. C.; Duan, H. Q.; Chen, Y. S. *J. Mater. Chem.* **2011**, *21*, 3448−3454.
(16) Zhang, L.; Xia, J.; Zhao, Q.; Liu, L.; Zhang, Z. *Small* **2010**, *6*, 537−544.
(17) Zhao, G.; Jiang, L.; He, Y.; Li, J.; Dong, H.; Wang, X.; Hu, W. *Adv. Mater.* **2011**, *23*, 3959−3963.
(18) Zhang, Y.; Tang, Z. R.; Fu, X.; Xu, Y. J. *ACS Nano* **2010**, *4*, 7303−7314.
(19) Yu, X. X.; Cai, H. B.; Zhang, W. H.; Li, X. J.; Pan, N.; Luo, Y.; Wang, X. P.; Hou, J. G. *ACS Nano* **2011**, *5*, 952−958.
(20) Huang, X.; Yin, Z.; Wu, S.; Qi, X.; He, Q.; Zhang, Q.; Yan, Q.; Boey, F.; Zhang, H. *Small* **2011**, *7*, 1876−1902.
(21) Huang, J.; Zhang, L.; Chen, B.; Ji, N.; Chen, F.; Zhang, Y.; Zhang, Z. *Nanoscale* **2010**, *2*, 2733−2738.
(22) Fu, X.; Bei, F.; Wang, X.; O'Brien, S.; Lombardi, J. R. *Nanoscale* **2010**, *2*, 1461−1466.
(23) Tjoa, V.; Jun, W.; Dravid, V.; Mhaisalkar, S.; Mathews, N. *J. Mater. Chem.* **2011**, *21*, 15593−15599.
(24) Zhang, Z.; Xu, F.; Yang, W.; Guo, M.; Wang, X.; Zhanga, B.; Tang, J. *Chem. Commun.* **2011**, *47*, 6440−6442.
(25) Ren, W.; Fang, Y.; Wang, E. *ACS Nano* **2011**, *5*, 6425−6433.
(26) Zhang, H.; Lu, G.; Li, H.; Liusman, C.; Yin, Z. Y.; Wu, S. X. *Chem. Sci.* **2011**, *2*, 1817−1821.
(27) Lu, L. H.; Liu, X. J.; Cao, L. Y.; Song, W.; Ai, K. L. *ACS Appl. Mater. Inter.* **2011**, *3*, 2944−2952.
(28) Kelemen, L. E. *Int. J. Cancer* **2006**, *119*, 243−250.
(29) Hu, S. H.; Chen, Y. W.; Hung, W. T.; Chen, I. W.; Chen, S. Y. *Adv. Mater.* **2012**, *24*, 1748−1754.
(30) Castillo, J. J.; R., T.; Novoa, L. V.; Svendsen, W. E.; Rozlosnik, N.; Boisen, A.; Escobar, P.; Martínez, F.; Castillo-León, J. *J. Mater. Chem. B* **2013**, *1*, 1475−1481.
(31) Mandal, S.; Bonifacio, A.; Zanuttin, F.; Sergo, V.; Krol, S. *Colloid Polym. Sci.* **2011**, *289*, 269−280.
(32) Georgakilas, V.; Otyepka, M.; Bourlinos, A. B.; Chandra, V.; Kim, N.; Kemp, K. C.; Hobza, P.; Zboril, R.; Kim, K. S. *Chem. Rev.* **2012**, *112*, 6156−6214.
(33) Pan, Y. Z.; Bao, H. Q.; Sahoo, N. G.; Wu, T. F.; Li, L. *Adv. Funct. Mater.* **2011**, *21*, 2754−2763.
(34) Guo, W. J.; Lee, R. J. *J. Controlled Release* **2001**, *77*, 131−138.
(35) Hummers, W. S.; Offeman, R. E. *J. Am. Chem. Soc.* **1958**, *80*, 1339−1339.
(36) Kovtyukhova, N. I.; Ollivier, P. J.; Martin, B. R.; Mallouk, T. E.; Chizhik, S. A.; Buzaneva, E. V.; Gorchinskiy, A. D. *Chem. Mater.* **1999**, *11*, 771−778.
(37) Zhang, X. K.; Meng, L. J.; Lu, Q. H.; Fei, Z. F.; Dyson, P. J. *Biomaterials* **2009**, *30*, 6041−6047.
(38) Pasricha, R.; Gupta, S.; Srivastava, A. K. *Small* **2009**, *5*, 2253−2259.
(39) Jasuja, K.; Berry, V. *ACS Nano* **2009**, *3*, 2358−2366.
(40) Xu, C.; Wang, X. *Small* **2009**, *5*, 2212−2217.
(41) Zhou, X. Z.; Huang, X.; Qi, X. Y.; Wu, S. X.; Xue, C.; Boey, F. Y. C.; Yan, Q. Y.; Chen, P.; Zhang, H. *J. Phys. Chem. C* **2009**, *113*, 10842−10846.
(42) Faria, A. F.; Martinez, D. S. T.; Moraes, A. C. M.; da Costa, M. E. H. M.; Barros, E. B.; Souza, A. G.; Paula, A. J.; Alves, O. L. *Chem. Mater.* **2012**, *24*, 4080−4087.
(43) Granatier, J.; Lazar, P.; Prucek, R.; Safarova, K.; Zboril, R.; Otyepka, M.; Hobza, P. *J. Phys. Chem. C* **2012**, *116*, 14151−14162.
(44) Hu, C. F.; Rong, J. H.; Cui, J. H.; Yang, Y. H.; Yang, L. F.; Wang, Y. L.; Liu, Y. L. *Carbon* **2013**, *51*, 255−264.
(45) Zhang, J. L.; Shen, G. X.; Wang, W. J.; Zhou, X. J.; Guo, S. W. *J. Mater. Chem.* **2010**, *20*, 10824−10828.
(46) Oh, J. M.; Choi, S. J.; Lee, G. E.; Han, S. H.; Choy, J. H. *Adv. Funct. Mater.* **2009**, *19*, 1617−1624.

(47) Stokes, R. J.; McBride, E.; Wilson, C. G.; Girkin, J. M.; Smith, W. E.; Graham, D. *Appl. Spectrosc.* **2008**, *62*, 371−376.
(48) Lok, C. N.; Ho, C. M.; Chen, R.; He, Q. Y.; Yu, W. Y.; Sun, H.; Tam, P. K.; Chiu, J. F.; Che, C. M. *J. Proteome Res.* **2006**, *5*, 916−924.
(49) Wigginton, N. S.; de Titta, A.; Piccapietra, F.; Dobias, J.; Nesatyy, V. J.; Suter, M. J.; Bernier-Latmani, R. *Environ. Sci. Technol.* **2010**, *44*, 2163−2168.
(50) Cui, J. H.; Hu, C. F.; Yang, Y. H.; Wu, Y. J.; Yang, L. F.; Wang, Y. L.; Liu, Y. L.; Jiang, Z. Y. *J. Mater. Chem.* **2012**, *22*, 8121−8126.
(51) Lu, W. T.; Senapati, D.; Wang, S. G.; Tovmachenko, O.; Singh, A. K.; Yu, H. T.; Ray, P. C. *Chem. Phys. Lett.* **2010**, *487*, 92−96.
(52) Sudimack, J.; Lee, R. J. *Adv. Drug Delivery Rev.* **2000**, *41*, 147−162.
(53) Choi, H.; Choi, S. R.; Zhou, R.; Kung, H. F.; Chen, I. W. *Acad. Radiol.* **2004**, *11*, 996−1004.
(54) Loh, K. P.; Bao, Q. L.; Eda, G.; Chhowalla, M. *Nat. Chem.* **2010**, *2*, 1015−1024.
(55) Pal, S.; Sharma, J.; Yan, H.; Liu, Y. *Chem. Commun.* **2009**, 6059−6061.
(56) Huang, P.; Bao, L.; Zhang, C. L.; Lin, J.; Luo, T.; Yang, D. P.; He, M.; Li, Z. M.; Gao, G.; Gao, B.; Fu, S.; Cui, D. X. *Biomaterials* **2011**, *32*, 9796−9809.
(57) Kneipp, K.; Kneipp, H.; Kneipp, J. *Acc. Chem. Res.* **2006**, *39*, 443−450.
(58) Anderson, N.; Anger, P.; Hartschuh, A.; Novotny, L. *Nano Lett.* **2006**, *6*, 744−749.
(59) Zavaleta, C. L.; Smith, B. R.; Walton, I.; Doering, W.; Davis, G.; Shojaei, B.; Natan, M. J.; Gambhir, S. S. *Proc. Nat. Acad. Sci. U.S.A.* **2009**, *106*, 13511−13516.
(60) Liu, Z. M.; Guo, Z. Y.; Zhong, H. Q.; Qin, X. C.; Wan, M. M.; Yang, B. W. *Phys. Chem. Chem. Phys.* **2013**, *15*, 2961−2966.
(61) Dieing, T.; Hollricher, O. *Vib. Spectrosc.* **2008**, *48*, 22−27.
(62) Wang, Z. Y.; Zong, S. F.; Yang, J.; Li, J.; Cui, Y. P. *Biosens. Bioelectron.* **2011**, *26*, 2883−2889.